Mitochondrial oxidative stress under hypoxia promotes gastric mucosal injury in portal hypertensive gastropathy

JIAJIE LUO, KAIDUAN XIE, XINGTONG OU and SIWEI TAN

Department of Gastroenterology, The Third Affiliated Hospital of Sun Yat-sen University, Guangzhou, Guangdong 510630, P.R. China

Received April 19, 2025; Accepted November 27, 2025

DOI: 10.3892/br.2026.2102

Abstract. Hypoxia, which represents a key pathological feature of gastric mucosal disorders, exacerbates mitochondrial oxidative stress through dysregulated cellular responses. However, the underlying mechanism of mitochondrial oxidative stress under hypoxia during gastric mucosal epithelial injury in portal hypertensive gastropathy (PHG) is not fully understood. To assess the impact of mitochondrial oxidative stress under hypoxic conditions during gastric mucosal epithelial injury in the PHG, mucosal tissues from patients with PHG and healthy individuals were collected. Furthermore, portal hypertension (PHT)-induced mouse PHG models and hypoxia-induced cell models were established. The roles of hypoxia-induced mitochondrial oxidative stress and glycolytic reprogramming in gastric mucosal epithelial injury were analysed. The findings demonstrated that mitochondrial oxidative stress is significantly elevated under hypoxic conditions, leading to an increase in reactive oxygen species (ROS) generation. This process contributes to gastric mucosal epithelial damage in both patients with PHG and mice with PHT. Notably, treatment with the ROS scavenger Mito-TEMPO reduced hypoxia-induced gastric mucosal injury in mice with PHT and mitigated cellular damage caused by hypoxia in a normal human gastric mucosal epithelial cell line (GES-1). Mitochondrial oxidative stress was shown to be associated with lactate dehydrogenase A upregulation, impaired ATP production and increased lactic acid release in gastric epithelial cells, all of which contribute to epithelial injury in the PHG. Therefore, hypoxia-induced mitochondrial oxidative stress has emerged as a promising therapeutic target for PHG.

Correspondence to: Professor Siwei Tan, Department of Gastroenterology, The Third Affiliated Hospital of Sun Yat-sen University, 600 Tianhe Road, Guangzhou, Guangdong 510630, P.R. China
E-mail: tansw@mail.sysu.edu.cn

Abbreviations: ATP, adenosine triphosphate; GES-1, human gastric mucosal epithelial cells; GO, Gene Ontology; H&E, hematoxylin and eosin; HIF-1α, hypoxia-inducible factor-1α; HK2, hexokinase-2; HRP, horseradish peroxidase; IHC, immunohistochemical; IF, immunofluorescence; LDHA, lactate dehydrogenase A; mtDNA, mitochondrial DNA; PBS, phosphate-buffered saline; PKM2, pyruvate kinase isozyme type M2; PHG, portal hypertensive gastropathy; PHT, portal hypertension; ROS, reactive oxygen species; TEM, transmission electron microscopy; VDAC, voltage-dependent anion channel; XO, xanthine oxidase; 4-HNE, 4-hydroxynonenal; 8-OHdG, 8-hydroxy-2'-deoxyguanosine

Key words: hypoxia, mitochondrial oxidative stress, glycolysis, LDHA, PHG

Introduction

Portal hypertensive gastropathy (PHG) has emerged as a serious clinical complication associated with portal hypertension (PHT). This condition manifests pathologically as congestive gastropathy, primarily resulting from compromised venous drainage in the gastric mucosal circulation (1,2). PHG predisposes patients to acute or chronic upper gastrointestinal bleeding, significantly compromising health outcomes and quality of life. The pivotal pathogenic determinant of PHG is elevated vascular resistance within the portal system, which drives PHT (3). PHT induces venous stasis within gastric circulation, mucosal congestion, and compromised tissue perfusion, culminating in hypoxia-mediated injury to gastric epithelial cells (4,5). Various pathway adaptations to hypoxic conditions, which trigger metabolic adaptations, modulate cell proliferation and oxidative capacity, and govern inflammatory responses, are instrumental in detecting low oxygen levels within cells. These hypoxia-responsive mechanisms have been pathologically associated with diverse disease processes, including neoplastic progression, cardiovascular pathophysiology, metabolic dysregulation syndromes, and gastrointestinal diseases (6,7). In addition, emerging evidence implicates that the pathogenesis of PHG is influenced by multifactorial mechanisms, such as dysregulation of cytokines (including endothelin-1, nitric oxide, prostaglandin E2, and tumour necrosis factor-α), epithelial apoptosis, disruption of the mucosal barrier, nonspecific inflammatory responses, and mitochondrial dysfunction (4,5). Nevertheless, the precise molecular pathogenesis remains incompletely elucidated, necessitating further systematic investigation.

Hypoxia induces structural and functional adaptations in mitochondria, which exacerbates oxidative stress and promotes anaerobic glycolysis (8). Mitochondria, the dominant source of reactive oxygen species (ROS) production, exhibit a close interplay between mitochondrial oxidative stress and

glycolytic dysfunction (9). ROS are frequently generated as byproducts during the process of oxidative phosphorylation. Effective regulation of ROS levels is crucial, as they can potentially induce oxidative damage to DNA, proteins, and lipids (10). Glycolysis, a highly conserved metabolic pathway, serves as the universal initial step in glucose metabolism. Under hypoxic conditions, glycolysis facilitates ATP generation through glucose catabolism, yielding lactic acid as the terminal metabolite (11). Increased ROS and excessive glycolysis can lead to alterations in cellular function and promote the occurrence of adverse events such as cell death. Our previous study has demonstrated that hypoxia-mediated mitochondrial dysfunction is a critical contributor to PHG pathogenesis (12). However, the potential causative role of hypoxia-induced ROS overproduction and accelerated glycolytic flux in the pathogenesis of PHG-associated mucosal injury remains to be systematically investigated.

Therefore, to elucidate the specific molecular mechanisms linking hypoxia-induced ROS accumulation and aberrant glycolytic metabolism in gastric epithelial injury in PHG, gastric mucosal biopsies from patients with PHG and healthy controls were analysed to identify transcriptomic and ultrastructural differences. A murine model of PHT via carbon tetrachloride administration and an *in vitro* model using hypoxia-exposed GES-1 were further established. Utilizing transmission electron microscopy (TEM), targeted metabolomics, and molecular assays, mitochondrial morphology, oxidative stress markers, and glycolytic flux were assessed. Additionally, the ROS scavenger Mito-TEMPO and the lactate dehydrogenase A (LDHA) inhibitor oxamic acid sodium were used to validate the therapeutic potential of targeting these pathways in preventing mucosal injury. The present study not only has the potential to reveal the key molecular links of the hypoxia-metabolism imbalance in PHG, but also to provide novel experimental evidence for the development of targeted therapeutic strategies against oxidative stress and abnormal glycolysis in PHG.

Materials and methods

Clinical tissue specimens. Gastric mucosal biopsy specimens were collected endoscopically from two groups: i) 10 patients diagnosed with PHG secondary to hepatitis B virus-related liver cirrhosis, with a mean age of 55.4±8.05 years, ranging from 43-70 years. Among these 10 patients, 5 (50.0%) were male and 5 (50.0%) were female; and ii) 10 healthy control subjects undergoing routine health examinations at the Endoscopic Center of the Third Affiliated Hospital of Sun Yat-sen University (Guangzhou, P.R. China) with a mean age of 53.6±7.74 years, ranging from 44-66 years. Among these 10 subjects, 5 (50.0%) were male and 5 (50.0%) were female. The study protocol was approved by the Clinical Research Ethics Committee of the Third Affiliated Hospital of Sun Yat-Sen University [approval no. (2021)02-176]. Gastric biopsy specimens, collected from both healthy controls and patients with PHG, underwent preservation either by freezing (-80˚C) for molecular biology applications or through formalin fixation/paraffin embedding for histopathological evaluation. Written informed consent from the patients was waived.

Mouse models. All animal experiments were conducted in accordance with protocols reviewed and approved (approval no. 2022F122) by the Institutional Animal Care and Use Committee of South China Agricultural University (Guangzhou, P.R. China) and conducted in accordance with relevant guidelines. Experimental groups were randomly assigned with 92 C57BL/6 mice (male, 6-8 weeks old, 18-20 g), which were maintained in a specific pathogen-free facility under standardized conditions (22±2˚C; 50-60% humidity; 12-h light/dark cycle). Mice were maintained in individually ventilated cages with sterilized wood-chip bedding and provided with autoclaved food and water *ad libitum*. All experimental procedures and assessments were performed in a blinded fashion. Following completion of experimental protocols, all mice were humanely euthanized via gradual-fill carbon dioxide asphyxiation, with a volume displacement rate of 70% utilized in our experimental procedures. Liver cirrhosis with subsequent PHT was induced in mice via twice-weekly intraperitoneal injections of carbon tetrachloride (20% v/v in olive oil; Sinopharm Chemical Reagent) at 5 ml/kg body weight for 16 weeks. Control mice received equivalent volumes of olive oil alone (5 ml/kg, intraperitoneally) on the same schedule. To mitigate oxidative stress, mice received intraperitoneal Mito-TEMPO (10 mg/kg solubilized in PBS; cat. no. HY-112879; MedChemExpress) every other day. Control groups were administered PBS alone at equivalent volumes and frequency. For LDHA suppression, oxamic acid sodium (750 mg/kg in PBS; HY-W013032A; MedChemExpress) was administered intraperitoneally every other day, with PBS serving as the vehicle control.

Sample collection. Mice from both the PHT and control groups were anesthetized with ketamine/xylazine (100 mg/kg and 10 mg/kg; intraperitoneal injection) and were humanely euthanized following anesthetic induction. Their abdomens were opened, and the entire stomach was carefully dissected. The stomach was repeatedly rinsed in ice-cold PBS solution to remove any residual contents, and then longitudinally cut along the greater curvature to expose the gastric mucosa. After thoroughly rinsing the gastric contents with ice-cold PBS, gross images were obtained, and the gastric mucosal injury was scored as follows (12): 0, normal gastric mucosa; 1, gastric mucosal erosion; 2, gastric mucosal ulcer (<1 mm); 3, gastric mucosal ulcer (1-2 mm); 4, gastric mucosal ulcer (3-4 mm); 5, gastric mucosal ulcer (>5 mm). Subsequently, the mucosal tissues were collected. A portion was stored in a -80˚C freezer for subsequent protein extraction. For paraffin section preparation, a separate portion was fixed in 10% neutral-buffered formalin.

Histopathological staining. Tissue sections (3-μm thick) were prepared for either hematoxylin and eosin (H&E) staining or immunohistochemical/immunofluorescence (IHC/IF) analyses. For immunostaining, antigen-retrieved tissue sections were incubated overnight at 4˚C with primary antibodies targeting either LDHA (cat. no. 19987-1-AP; Proteintech Group, Inc.) or 4-HNE (cat. nos. ab46545/ab48506; Abcam), followed by incubation with species-matched horseradish peroxidase (HRP)-conjugated secondary antibodies (cat. nos. A0208/A0216; Beyotime Institute of Biotechnology)

at 37˚C for 1.5 h, as previously described (13). IF sections were DAPI-counterstained to visualize nuclei. Tissue hypoxia distribution was evaluated in gastric mucosal sections using the Hypoxyprobe-1 Kit (cat. no. HP3-100Kit; Hypoxyprobe, Inc.) following the manufacturer's protocol. Briefly, 1 h before anesthetization and sampling, mice were intraperitoneally injected with a Hypoxyprobe-1 solution at a dose of 60 mg/kg. Subsequently, the samples underwent fixation, embedding, and sectioning into 3 μm-thick slices. After incubation with the IgG1 monoclonal antibody (MAb1; clone 11.23.22.R; supplied in the Hypoxyprobe-1 Kit, cat. no. HP3-100Kit; Hypoxyprobe, Inc.) at 4˚C overnight, the sections were incubated with HRP-labeled anti-rat secondary antibodies (cat. no. A0192; Beyotime Institute of Biotechnology) at room temperature for 1.5 h, followed by DAB staining. For primary cells, they were first incubated with a 100-μM Hypoxyprobe-1 solution for 1 h, and then subjected to permeabilization with 0.3% Triton X-100 for 20 min at room temperature (cat. no. P0096; Beyotime Institute of Biotechnology). After incubating with the IgG1 MAb1 at 4˚C overnight, the cells were stained with anti-rat secondary antibodies (cat. no. A-11006; Thermo Fisher Scientific, Inc.) at 37˚C for 1 h. Nuclei were counterstained with DAPI for 15 min at room temperature prior to imaging. The quantitative analysis of Hypoxyprobe-1-positive regions was performed in multiple fields of view (>6 per sample). The ratio of positive regions to the total area in each image was quantified using ImageJ software (v1.54 g; National Institutes of Health), and the area ratio was calculated and expressed as a percentage. For TEM detection, fresh gastric tissue samples were immediately fixed in electron microscope fixative (cat. no. LADE035; LANDM Biotechnology Co., Ltd.; Guangzhou Ruijing Information Technology Co., Ltd.) at 4˚C overnight (or for at least 4 h). The samples were dehydrated in a graded ethanol series (50-100%) followed by 100% acetone, infiltrated, and embedded in resin (polymerized at 60˚C for 48 h). Ultrathin sections (~100 nm) were cut using a Leica UC7 ultramicrotome. Sections were stained with uranyl acetate (cat. no. U25690; Shanghai Acmec Biochemical Technology Co., Ltd.) for 20 min and lead citrate (cat. no. L885990; Macklin, Inc.) for 12 min at room temperature and imaged using a transmission electron microscope (Tecnai G2 Spirit; FEI). Mitochondrial morphometric analysis was performed by randomly selecting eight mitochondria per image from each experimental group. Mitochondrial length and width were quantified using length parameters, while cross-sectional area was calculated via area measurement tools.

Cell experiments. For the isolation of primary cells (14), the intact stomach was meticulously excised and subsequently rinsed with a physiological buffer. The pyloric region was securely ligated. Following this, the stomach was perfused via the cardia using calcium-free Hank's Balanced Salt Solution for a duration of 15 min to facilitate tissue preparation. Following the initial perfusion, the stomach was subjected to further enzymatic digestion by perfusion with 100 ml of a digestion solution containing 0.2% pronase and 0.2% collagenase type IV (both from Sigma-Aldrich; Merck KGaA). After enzymatic treatment, the mucosal layer was carefully dissected and collected to generate a single-cell suspension. The resulting suspension was then passed through a 100-μm nylon mesh filter to remove undigested tissue fragments and ensure a homogeneous cell population. The cell suspension was centrifuged at 300 x g for 15 min to separate cellular components. Following centrifugation, the resulting pellet was carefully harvested for subsequent isolation of gastric epithelial cells. A 30% Percoll solution (Sigma-Aldrich; Merck KGaA) was prepared according to the manufacturer's protocol. The cellular pellet was then carefully layered onto the Percoll density gradient and centrifuged at 450 x g for 20 min at 4˚C to isolate viable gastric epithelial cells. Primary cells were maintained in RPMI-1640 medium (cat. no. 11875093; Thermo Fisher Scientific, Inc.) supplemented with 10% heat-inactivated fetal bovine serum (cat. no. A5256701; Thermo Fisher Scientific, Inc.) and antibiotic-antimycotic solution (cat. no. 15240062; Thermo Fisher Scientific, Inc.). Incubation was carried out at 37˚C in a humidified chamber with 5% CO_2 tension. For comparative purposes, the GES-1 human gastric epithelial cell line was grown under identical conditions, as previously established (15). For the hypoxia group, the cells were switched to low-glucose culture medium and incubated in a tri-gas incubator (1% oxygen, 5% CO_2, 94% nitrogen) for 24 h. The normoxia group was cultured in normal medium in a CO_2 incubator for 24 h. The working concentrations of Mito-TEMPO and oxamic acid sodium were both set at 10 μmol/l. Using the Cell Counting Kit-8 (CCK-8; cat. no. C0038; Beyotime Institute of Biotechnology) assay, cellular viability across experimental groups was systematically measured and compared after incubating the cells with the reagent for 1.5 h at 37˚C as per the manufacturer's instructions.

Western blotting. Total protein extracts from mucosal tissues or isolated cells were subjected to western blot analysis following established protocols (14,15). These protein extracts were obtained using a total protein extraction kit (cat. no. PC201; Shanghai EpiZyme Biomedical Technology Co., Ltd.). Protein concentration was determined using the BCA protein assay kit (cat. no. ZJ102; Shanghai EpiZyme Biomedical Technology Co., Ltd.). A total of 20 μg of protein was loaded per lane and separated on a 10% SDS-PAGE gel. Proteins were subsequently transferred to a polyvinylidene difluoride membrane. The membrane was blocked with 5% milk in TBST at room temperature for 1.5 h. Washing was performed three times for 5 min each, using TBST containing 0.1% Tween-20. Membranes were incubated overnight at 4˚C with primary antibodies against LDHA (cat. no. 19987-1-AP; Proteintech Group, Inc.) and β-actin (cat. no. sc-47778; Santa Cruz Biotechnology, Inc.), with β-actin serving as the loading control. Protein bands were detected using enhanced chemiluminescence (ECL; cat. no. E423-02; Vazyme Biotech Co., Ltd.) after HRP-secondary antibody incubation (cat. no. RM3001/3002, Beijing Ray Antibody Biotech) for 1 h at room temperature. Signal acquisition was performed digitally, with band intensity quantification conducted using ImageJ (v1.54 g; National Institutes of Health).

ATP measurement. Gastric tissues (20 mg) were homogenized in 200 μl of the ATP detection lysis buffer supplied with the Enhanced ATP Assay Kit (cat. no. S0027; Beyotime Institute of Biotechnology) using the Bead Ruptor 12 Homogenizer

(Omni International, Inc.). The homogenates were centrifuged (12,000 x g, 5 min, 4˚C), and the supernatant was collected. Protein concentration was determined using a BCA Protein Assay Kit (cat. no. ZJ102; Shanghai EpiZyme Biomedical Technology Co., Ltd.). Subsequently, a 20-μl aliquot of the supernatant was mixed with 100 μl of the ATP detection working solution, and luminescence (RLU) was measured using a microplate luminometer (Agilent BioTek Synergy H1 Microplate Reader; Agilent Technologies, Inc.) with a 2 sec delay and 10 sec integration time. ATP concentrations were calculated based on a standard curve (0, 2.5, 5, 10, 20, 40, and 50 μM) and normalized to protein concentration (nmol/mg protein). Samples and standards were run in triplicate.

Microarray analysis. The microarray experiment followed the same protocol as previously described (14). The microarray experiment was performed using the Agilent SurePrint G3 Human Gene Expression Microarray 8x60K platform (G4851B; Agilent Technologies, Inc.). Total RNA quality and quantity were assessed via Agilent 2100 Bioanalyzer; samples with an RNA Integrity Number (RIN) ≥7.0, concentration ≥50 ng/μl, and 28S/18S ratio ≥1.8 were used. Labeling was conducted using the Agilent Low Input Quick Amp Labeling Kit (part no. 5190-2305; Agilent Technologies, Inc.) following the manufacturer's protocol. Briefly, double-stranded cDNA was synthesized using AffinityScript Reverse Transcriptase (supplied in the Agilent Low Input Quick Amp Labeling Kit; part no. 5190-2305; Agilent Technologies, Inc.) and a T7 promoter primer (supplied in the Agilent Low Input Quick Amp Labeling Kit; part no. 5190-2305; Agilent Technologies, Inc.). This was followed by *in vitro* transcription (IVT) with T7 RNA Polymerase at 37˚C for 14 h to generate cRNA labeled with Cy3-CTP. Hybridization was carried out in an Agilent hybridization oven (Model G2545A; Agilent Technologies, Inc.) at 65˚C for 17 h using the Agilent Gene Expression Hybridization Kit (part no. 5188-5242; Agilent Technologies, Inc.). Subsequent data processing was conducted with GeneSpring GX version 12.0 (Agilent Technologies, Inc.), which executed data aggregation and normalization procedures. Differential gene expression analysis employed the following selection criteria: i) Absolute value of expression ratio ≥1.5-fold; ii) statistical significance threshold set at P<0.05 after Benjamini-Hochberg false discovery rate adjustment. The expression data were log2-transformed and hierarchically clustered via CLUSTER 3.0 (http://bonsai.hgc.jp/~mdehoon/software/cluster/) Adjust Data function. Subsequently, the resulting dendrogram was visualized with Java TreeView (v1.2.1; http://jtreeview.sourceforge.net/) for further analysis. Gene Ontology (GO) enrichment analysis was performed using the clusterProfiler R package (v4.14.6; https://bioconductor.org/packages//release/bioc/html/clusterProfiler.html). GO terms with an adjusted P-value <0.05 were considered statistically significant. The results were visualized using bubble plots.

Energy metabolic analysis. Energy metabolism was profiled using a targeted metabolomics platform [UPLC-MS/MS; Metabo-Profile Biotechnology (Shanghai) Co., Ltd.] on gastric tissue. Specifically, 10 mg of frozen sample was homogenized with ultrapure water and ceramic grinding beads (cat. no. F6632; Beyotime Institute of Biotechnology), and then extracted using methanol containing internal standards. The samples were centrifuged at 18,000 x g for 15 min at 4˚C (Microfuge 20R; Beckman Coulter, Inc.). Following centrifugation, metabolites were derivatized with 3-nitrophenylhydrazine and 1-ethyl-3-(3-dimethylaminopropyl) carbodiimide at 30˚C for 60 min. Chromatographic separation was performed on a BEH C18 column (2.1x100 mm, 1.7 μm; 40˚C) with a gradient of mobile phase A (5 mM DIPEA aqueous solution) and mobile phase B (acetonitrile/isopropanol, 7:3, v/v) at 0.3 ml/min. MS detection was carried out in negative ESI mode (capillary voltage, 3 kV; source temperature: 150˚C; desolvation temperature, 500˚C). Data were acquired on a Waters ACQUITY I UPLC/Xevo TQ-S system and processed with MassLynx (v4.1; Waters Corporation). Metabolite levels were normalized to sample weight, and missing values were imputed as one tenth of the minimum for each metabolite. Subsequent analyses, including principal component analysis (PCA) and orthogonal partial least squares discriminant analysis (OPLS-DA), were performed using iMAP [v1.0; Metabo-Profile Biotechnology(Shanghai) Co., Ltd.]. Differentially expressed metabolites were identified based on variable importance in projection ≥1 (from OPLS-DA) and P<0.05 from univariate tests.

Determination of oxidative stress. Cellular ROS production was assessed using DCFH-DA (cat. no. S0033S; Beyotime Institute of Biotechnology). The primary gastric epithelial cells were cultured to approximately 60-70% confluence and subjected to the treatments. Subsequently, the cells were incubated with DCFH-DA (diluted 1:1,000 in RPMI-1640 medium) for 20 min at 37˚C. After probe incubation, oxidative conversion to fluorescent DCF was measured at 488/525 nm excitation/emission. Mitochondrial superoxide was assessed by seeding cells in confocal dishes overnight. Cells were then stained with 5 μM MitoSOX™ Red (cat. no. M36008; Thermo Fisher Scientific, Inc.) at 37˚C for 20 min (in the dark). Subsequently, the cells were gently washed three times with warm PBS, followed by Hoechst 33258 (cat. no. C1017; Beyotime Institute of Biotechnology) nuclear counterstaining at room temperature for 20 min for localization. Fluorescence imaging was performed using a Zeiss LSM880/800 confocal microscope (Imager Z2; Zeiss AG). Mitochondrial DNA (mtDNA) was extracted with the AllPrep DNA/RNA Mini Kit (cat. no. 80204; Qiagen) from the mitochondrial fraction of cells, and oxidative damage was assessed via 8-hydroxy-2'-deoxyguanosine (8-OHdG) quantification using the OxiSelect™ Oxidative DNA Damage ELISA Kit (cat. no. STA-320; Cell Biolabs, Inc.). Prior to the assay, extracted mtDNA samples were dissolved and normalized to a uniform concentration of 1 mg/ml. Following enzymatic digestion, a total of 50 μg of processed mtDNA was loaded per reaction (50-μl volume). The 8-OHdG content was determined by comparison with a predetermined standard curve (0-20 ng/ml) and is reported as ng/ml.

Statistical analysis. All results were consistently reproduced in at least three independent experiments. Representative data from distinct biological replicates were selected for visualization in figures (for example microscopy images, immunoblots). Quantitative data are reported as the mean ± standard error

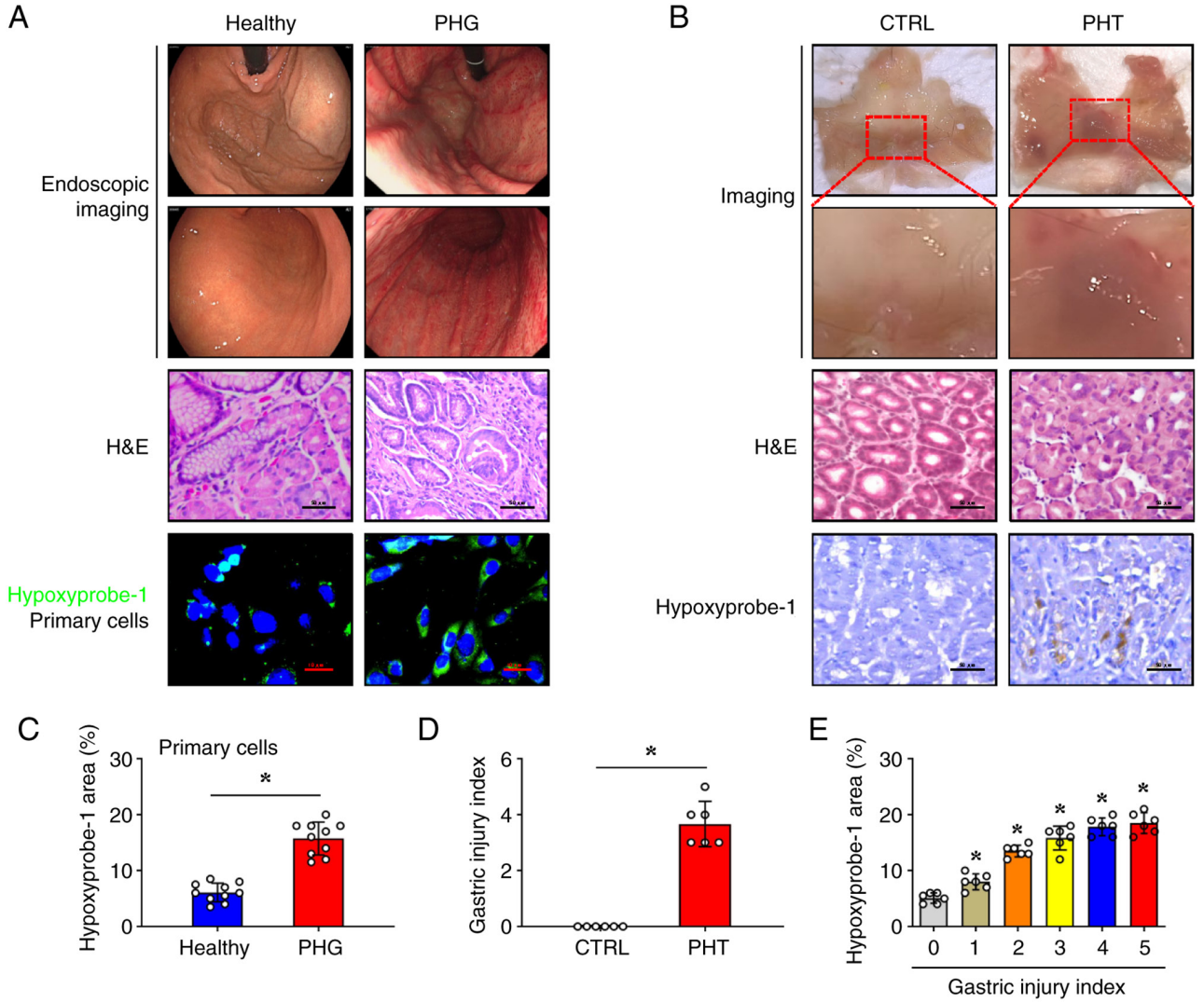

Figure 1. Hypoxia participates in gastric mucosal injury of PHG in both humans and mice. (A) Representative gastric endoscopic images and H&E-stained sections of gastric mucosa from patients with PHG were compared with those from healthy individuals (as Healthy). Scale bar, 50 μm for H&E images. Hypoxyprobe-1 staining (green) was performed on primary gastric mucosal epithelial cells isolated from both PHG patients and healthy controls. Nuclei (blue) were counterstained with DAPI. Scale bar, 10 μm. (B) Gross image, H&E staining, and Hypoxyprobe-1 immunohistochemical staining (brown) of the gastric mucosa in the mice with PHT compared with that in the control mice. Scale bar, 50 μm for H&E and IHC images. (C) Quantitative analysis of Hypoxyprobe-1 fluorescence intensity from (A), n=10 per group; *P<0.05. (D) Mucosal injury index analysis in the murine models is presented, n=6 per group; *P<0.05. (E) The percentage of the Hypoxyprobe-1-positive area corresponding to the gastric injury index of PHT mouse models was analyzed. n=6 per group; *P<0.05 vs. the group with a gastric injury index of 0. PHG, portal hypertensive gastropathy; H&E, hematoxylin and eosin; DAPI, 4',6-diamidino-2-phenylindole dihydrochloride; PHT, portal hypertension; CTRL, control.

of the mean (SEM). All statistical analyses were conducted using GraphPad Prism software (version 9.5; Dotmatics). Comparisons between two groups were analyzed using Student's two-tailed paired *t*-test. Comparisons of single-factor data among more than two groups were analyzed using one-way analysis of variance (ANOVA), while comparisons of two-factor data among more than two groups were analyzed using two-way ANOVA. When the F-value was <0.05, Bonferroni's post hoc multiple comparison test was performed. A value of P<0.05 was considered to indicate a statistically significant difference.

Results

Hypoxia participates in the gastric mucosal injury of PHG in both humans and mice. To evaluate hypoxia in PHG pathogenesis, gastric mucosal biopsies were obtained from patients who had PHG confirmed by endoscopy, and a murine PHG model induced by PHT was developed. Endoscopic assessment demonstrated significant mucosal abnormalities in patients with PHG, including diffuse erythema, vascular congestion, and oedema, which were absent in healthy controls (Fig. 1A). Histopathological analysis of gastric mucosal biopsies using H&E staining demonstrated epithelial cell damage, focal haemorrhages, and submucosal venular ectasia in the PHG group (Fig. 1A). Hypoxyprobe-1 fluorescence signals were significantly enhanced in primary gastric mucosal epithelial cells isolated from these tissues in the PHG group (Fig. 1A and C). In the PHT mouse model, gross examination showed marked mucosal congestion and even erosive haemorrhage (Fig. 1B). Similar to the clinical samples from the PHG group, the mice with PHT exhibited significant epithelial

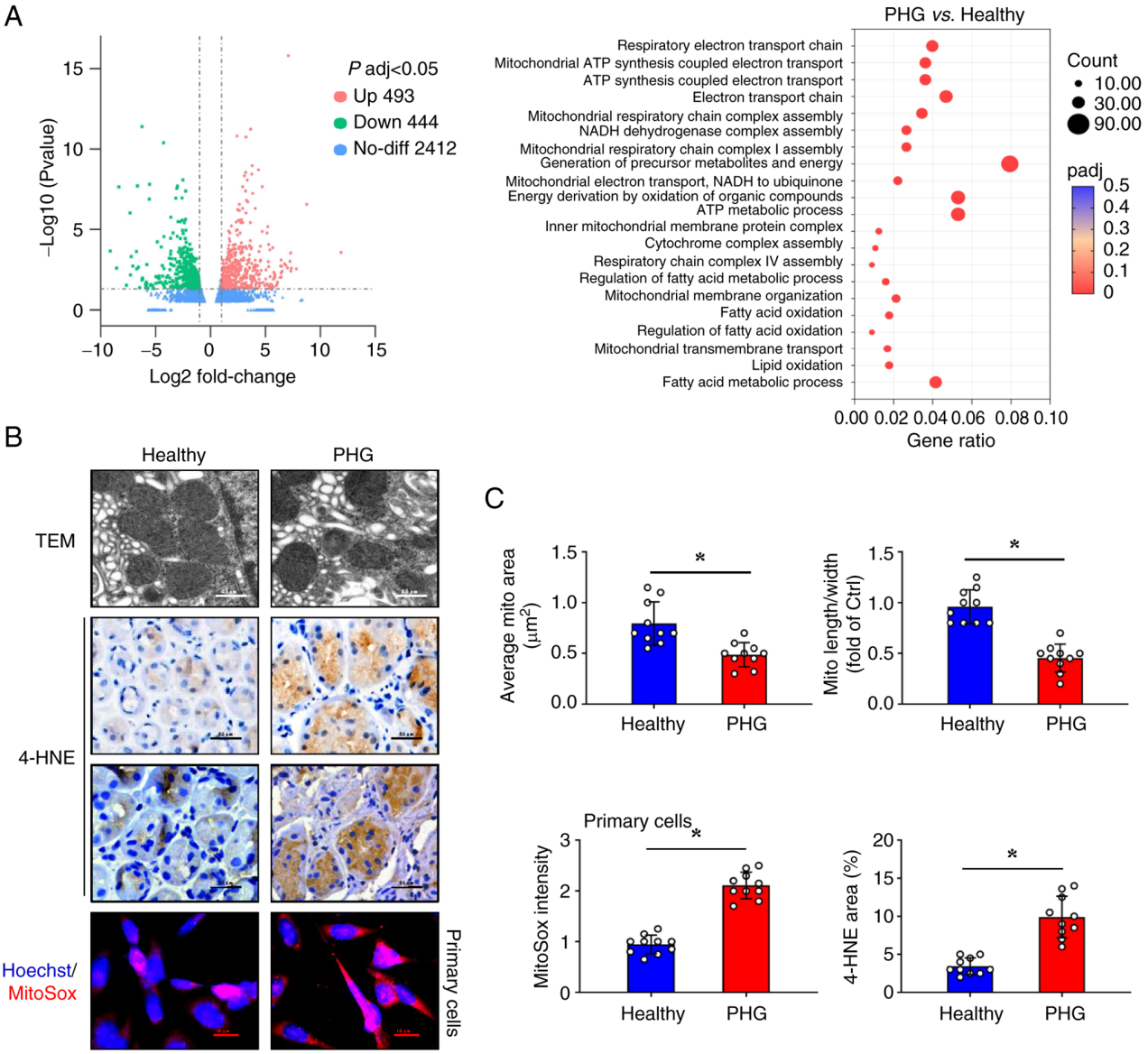

Figure 2. Enhanced mitochondrial oxidative stress is identified in the gastric mucosa epithelia of patients with PHG. (A) Volcano plot of differentially expressed genes in the PHG group compared with those in the healthy individual group. GO pathway enrichment of signalling pathways according to the microarray analysis, n=3 in each group. (B) TEM analysis of mitochondrial morphological changes (Scale bar, 0.5 μm), 4-HNE immunohistochemical staining (Scale bar=50 μm), and MitoSox fluorescent staining of primary gastric mucosal epithelial cells were performed in the gastric mucosal tissues from both healthy individuals (as Healthy) and patients with PHG (as PHG). Nuclei (blue) were counterstained with Hoechst 33258 in fluorescence staining. Scale bar, 10 μm. (C) The quantitative values of mitochondrial average area and mitochondrial length-to-width ratio obtained from TEM were presented. The MitoSox fluorescence intensity and 4-HNE staining quantification from (B) were also determined, n=10 per group; *P<0.05. PHG, portal hypertensive gastropathy; GO, Gene Ontology; TEM, transmission electron microscopy.

cell damage, which was associated with an elevated mucosal injury index (Fig. 1B and D). Moreover, the Hypoxyprobe-1 signal in the PHT group was enhanced, which was positively associated with the gastric injury index of mice with PHT (Fig. 1B and E). Collectively, these findings demonstrated that hypoxia serves as a pathogenic factor contributing to gastric mucosal injury in PHG.

Enhanced mitochondrial oxidative stress is identified in the gastric mucosa epithelia of PHG. To characterize the molecular alterations in PHG pathogenesis, microarray analysis was conducted on gastric mucosal biopsies obtained from both patients with PHG and healthy control subjects. Comparative transcriptomic analysis revealed significant differential gene expression profiles between PHG and normal gastric mucosa (Fig. 2A). Furthermore, Gene Ontology (GO) enrichment analysis demonstrated upregulation of mitochondrial structural components (including 'mitochondrial respiratory chain complex assembly', 'NADH dehydrogenase complex assembly', 'inner mitochondrial membrane protein complex', and 'mitochondrial membrane organization') and oxidative respiration (including 'generation of precursor metabolites and energy', 'energy derivation by oxidation of organic compounds', 'respiratory electron transport chain', and 'mitochondrial ATP synthesis coupled electron transport') in PHG specimens (Fig. 2A). TEM analysis identified ultrastructural mitochondrial abnormalities in the PHG mucosa, including reduced mitochondrial size and decreased mitochondrial

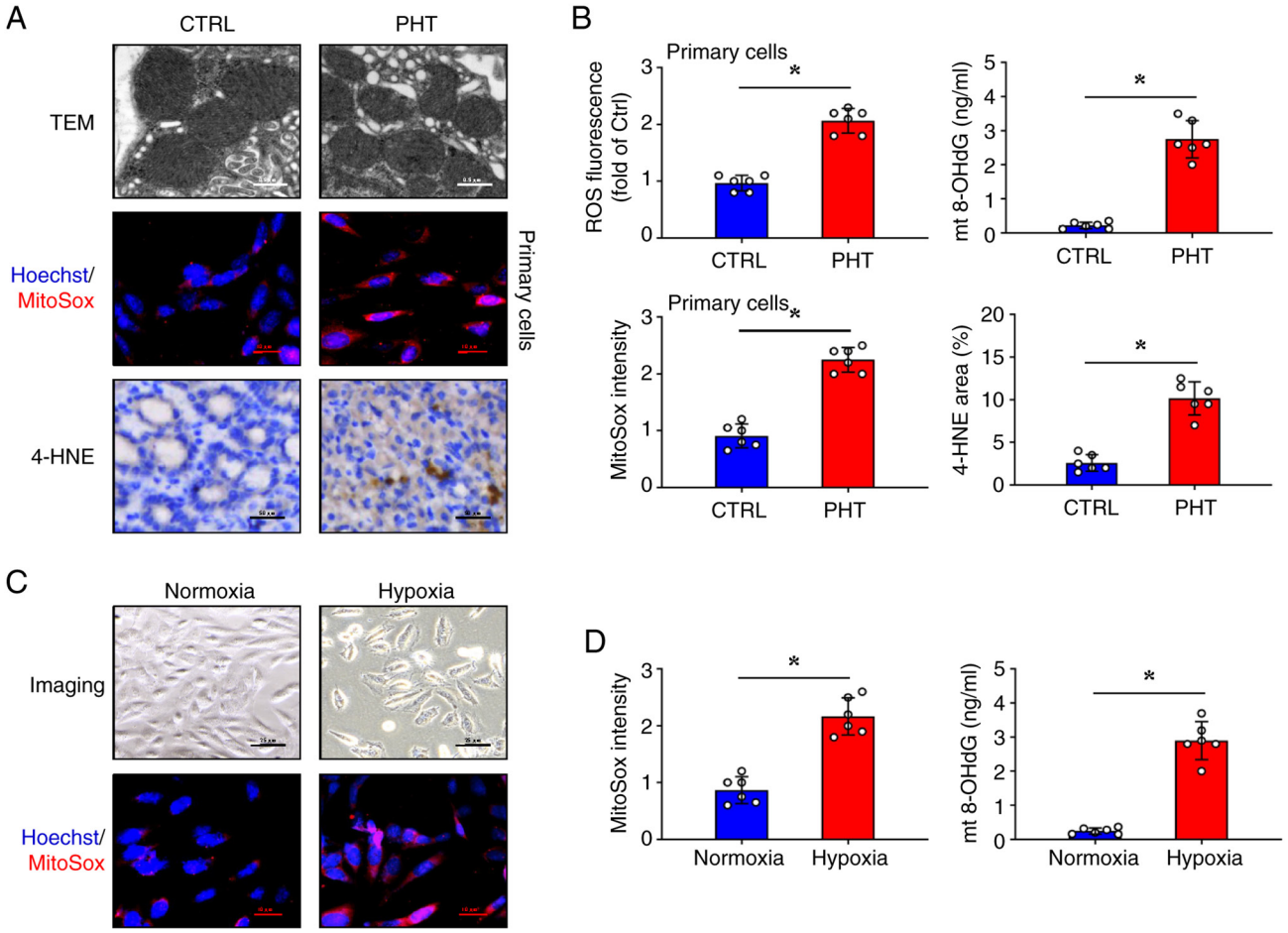

Figure 3. Mitochondrial oxidative stress is enhanced in the *in vivo* and *in vitro* models. (A) TEM analysis of mitochondrial morphological changes (Scale bar, 0.5 μm), MitoSox staining of primary gastric mucosal epithelial cells (Scale bar, 10 μm), and immunohistochemical staining for 4-HNE were performed in the gastric mucosal tissues from both control and PHT group mice (Scale bar, 50 μm). Nuclei (blue) were counterstained with Hoechst 33258 in MitoSox staining. (B) The quantitative analysis of ROS fluorescence in primary gastric mucosal epithelial cells and mt 8-OHdG concentration were determined. The MitoSox fluorescence intensity and the quantitative analysis of 4-HNE staining from (A) were also analyzed. n=6 per group; *P<0.05. (C) Morphology and MitoSox fluorescence staining of GES-1 cells under normoxic and hypoxic conditions. Nuclei (blue) were counterstained with Hoechst 33258 in MitoSox staining. Scale bars, 25 μm (upper panels) and 10 μm (lower panels). (D) The mt 8-OHdG concentration and the quantitative analysis of MitoSox fluorescence intensity in GES-1 cells under normoxic and hypoxic conditions are shown. n=6 per group; *P<0.05. TEM, transmission electron microscopy; PHT, portal hypertension; mt 8-OhdG, mitochondrial 8-OhdG; CTRL, control.

cristae. The quantitative assessment indicated decreases in the mean mitochondrial area as well as the length-to-width ratio (Fig. 2B and C). Immunohistochemical staining showed that PHG tissues had elevated expression of 4-HNE, a lipid peroxidation marker (Fig. 2B and C). Consistently, primary gastric epithelial cells from patients with PHG exhibited stronger MitoSox fluorescence signals than those from healthy controls (Fig. 2B and C), indicating increased mitochondrial superoxide production. PHT mouse models were established, and it was verified that TEM analysis of gastric mucosa from mice with PHT recapitulated clinical findings, demonstrating mitochondrial shrinkage, damage, and cristae loss compared with the control mice (Fig. 3A). In addition to the increased MitoSox signalling and increased intracellular ROS levels in the primary gastric epithelial cells, in mice with PHT, the gastric mucosa also exhibited significantly increased 4-HNE expression and elevated mitochondrial 8-OHdG (mt 8-OHdG) concentrations (Fig. 3A and B). Furthermore, the effects of hypoxia were explored on the human gastric epithelial cell line (GES-1) at the cellular level. Significant morphological changes were observed in GES-1 cells under hypoxic conditions compared with the controls, including reduced cell volume, enlarged central pale areas, and increased cell death (Fig. 3C). Enhanced MitoSox signals and increased mt 8-OHdG concentrations demonstrated that hypoxia induced mitochondrial oxidative stress in GES-1 cells (Fig. 3C and D). In summary, these findings indicated that mitochondrial structural alterations and oxidative stress escalation observed in the gastric mucosa contribute to the pathogenesis of PHG.

Mito-TEMPO attenuates gastric mucosal epithelial damage in in vivo and in vitro models. The ROS scavenger Mito-TEMPO, which is an antioxidant targeted to mitochondria, was used to investigate the therapeutic potential of mitochondrial oxidative stress inhibition (12). H&E staining revealed that Mito-TEMPO relieved gastric mucosal injury, with decreased inflammatory cell infiltration and attenuated capillary dilation in mice with PHT (Fig. 4A). However, no significant differences were

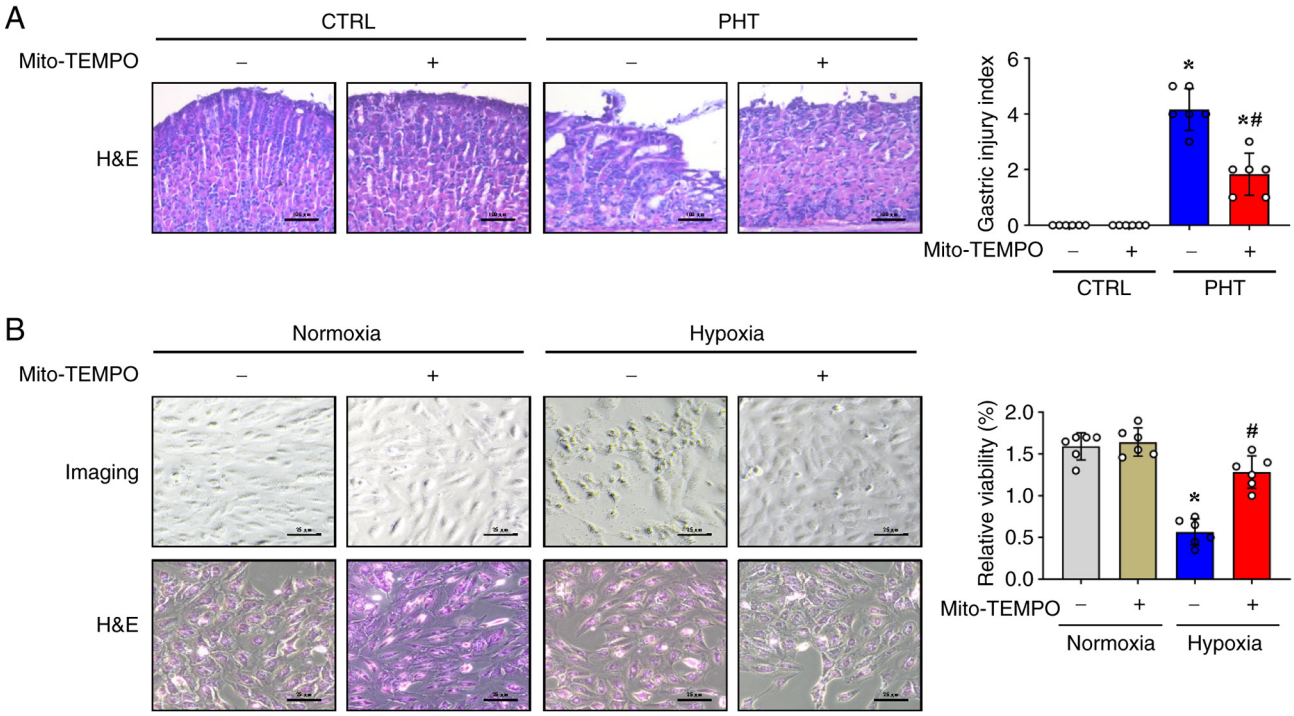

Figure 4. ROS scavenger Mito-TEMPO attenuates gastric mucosal epithelial injury from *in vivo* and *in vitro* models. (A) H&E staining of gastric mucosal tissues and analysis of gastric mucosal injury index in the mouse model treated with Mito-TEMPO or not. Scale bar, 100 μm. n=6 per group. *P<0.05 vs. the control group; $^{\#}$P<0.05 vs. the PHT group without Mito-TEMPO. (B) The morphology and H&E staining of GES-1 cell under normoxic and hypoxic conditions treated with Mito-TEMPO (or not) are shown. The relative cell viability analyzed by Cell Counting Kit-8 were also determined. Scale bar, 25 μm. n=6 per group. *P<0.05 vs. the normoxia group; $^{\#}$P<0.05 vs. the hypoxia group without Mito-TEMPO. ROS, reactive oxygen species; H&E, hematoxylin and eosin; PHT, portal hypertension; CTRL, control.

observed in the gastric mucosa of control mice treated with or without Mito-TEMPO (Fig. 4A). Furthermore, when used in the *in vitro* cell model under normoxic and hypoxic conditions, histological and cell viability analyses revealed that Mito-TEMPO was able to restore the morphological alterations and increase the relative cell viability in GES-1 cells under hypoxic conditions (Fig. 4B), and Mito-TEMPO did not affect the status of GES-1 cells under normoxic conditions (Fig. 4B). These findings demonstrated that mitochondrial-derived oxidative stress contributes to both PHT-induced gastric mucosal damage and hypoxic cellular injury. Notably, the mitochondrial-targeted antioxidant Mito-TEMPO alleviated these pathological changes in murine models and *in vitro* systems.

Mitochondrial oxidative stress is associated with LDHA upregulation, which impairs ATP production and promotes lactic acid production. Microarray analysis of clinical gastric mucosal biopsies revealed significant differential expression of glycolytic pathway-related genes between patients with PHG and healthy controls. Moreover, the expression of glycolysis-related genes in the glycolytic metabolic pathway, such as *hexokinase-2* (*HK2*), *LDHA*, and *pyruvate kinase isozyme type M2* (*PKM2*), was increased in the gastric mucosa of patients with PHG (Fig. 5A). Genomic metabolic pathway analysis confirmed the enrichment of genes that were differentially expressed in the glycolytic process, with LDHA exhibiting the most pronounced increase in transcription (Fig. 5B and C). Histological staining revealed that the protein expression of LDHA was consistent with the results of microarray analysis and was significantly upregulated in the patients with PHG and the mice with PHT (Fig. 5D). Moreover, the protein expression of LDHA increased in the GES-1 cell model following hypoxia (Fig. 5D). Furthermore, western blot analysis revealed a similar trend in LDHA expression in the three different sections (Fig. 5E). These findings established that mitochondrial dysfunction may drive LDHA upregulation to facilitate glycolytic adaptation to bioenergetic stress under hypoxia.

Given the established roles of mitochondrial oxidative stress in PHG pathogenesis and hypoxia-induced LDHA upregulation in glycolytic reprogramming, energy metabolic analysis of gastric mucosal tissues was performed to systematically characterize the associated metabolic alterations. Distinct clustering patterns were observed between the PHT and control groups using PCA (Fig. 6A). Metabolomic profiling revealed significant alterations in gastric mucosal metabolism, with mice with PHT exhibiting elevated organic acid metabolism and reduced carbohydrate metabolism compared with the control mice (Fig. 6B). Among these findings, the increase in the lactic acid concentration was the most significant (Fig. 6C). Because increased glycolysis can inhibit normal cellular aerobic oxidation and lead to reduced ATP production, the ATP levels were assessed and it was revealed that ATP levels were decreased in samples from patients with PHG, mice with PHT, and hypoxic GES-1 cells (Fig. 6D), whereas lactic acid concentrations were elevated in these groups (Fig. 6E). The LDHA inhibitor oxamic acid sodium alleviated the gastric

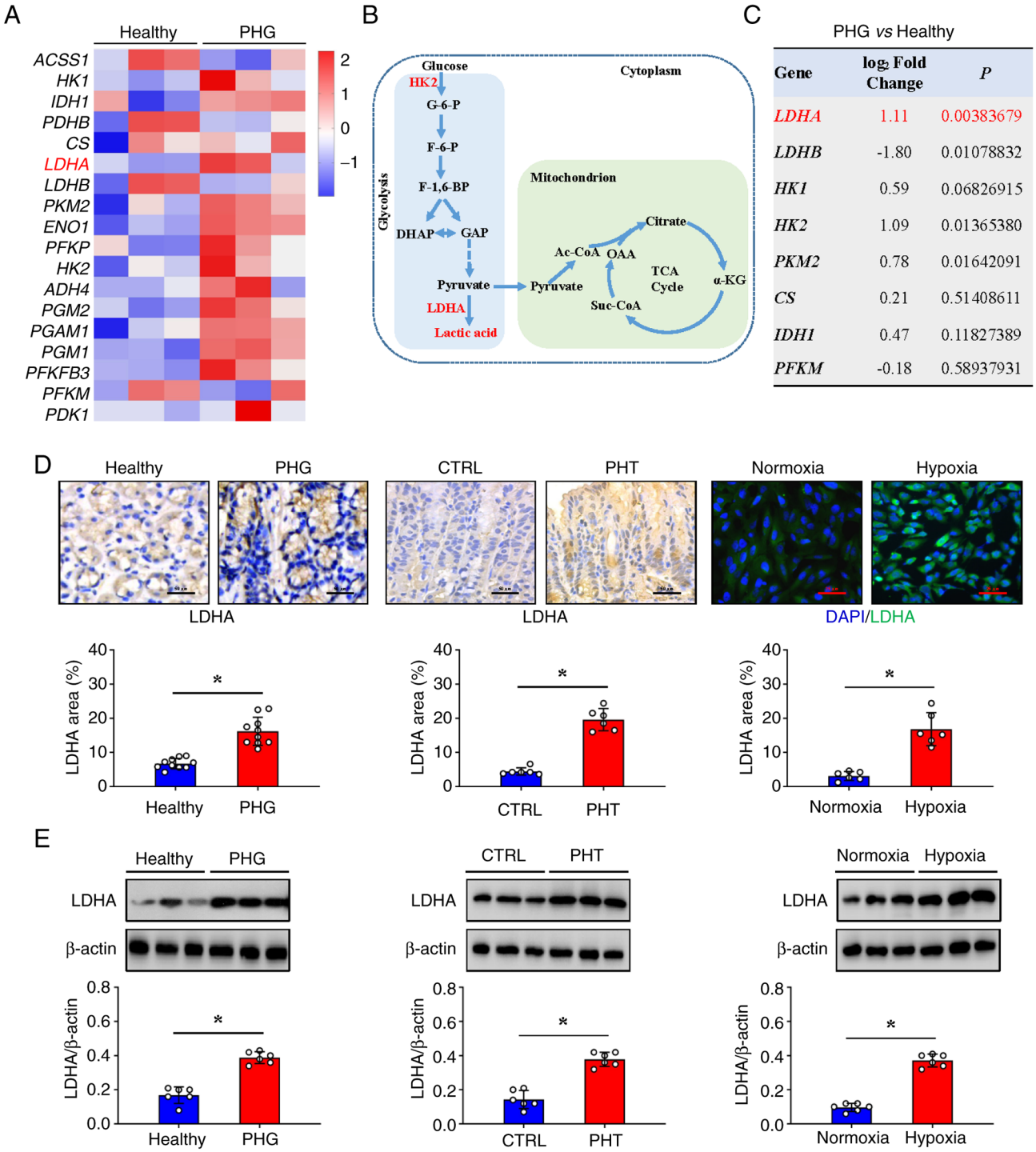

Figure 5. Mitochondrial dysfunction is associated with the glycolytic LDHA upregulation in PHG. (A) The heatmap analysis of differentially expressed genes between normal gastric mucosa (healthy individuals-indicated as Healthy) and gastric mucosa from patients with PHG (indicated as PHG) revealed increased expression of LDHA and other genes involved in the glycolytic metabolic pathway. (B) The glycolytic metabolic pathway is presented. (C) The fold changes and P-values of the indicated mRNAs in PHG tissues relative to those in normal (healthy individuals-indicated as Healthy) tissues from the microarray experiment are presented. (D) Immunohistochemical (brown) or immunofluorescence (green) staining and quantitative analysis of LDHA in the clinical tissue samples (n=10 per group), mouse models (n=6 per group), and cellular hypoxia models (n=6 per group). Nuclei (blue) were counterstained with DAPI in immunofluorescence staining. Scale bars, 50 μm (IHC images) and 25 μm (IF images). *P<0.05. (E) Western blotting detection of LDHA protein expression levels in clinical tissue samples, mouse models, and cellular hypoxia models. Ratios of densitometric units of normalized LDHA/β-actin were determined from western blotting. n=6 per group. *P<0.05. PHG, portal hypertensive gastropathy; LDHA, lactate dehydrogenase A; DAPI, 4',6-diamidino-2-phenylindole dihydrochloride; CTRL, control; PHT, portal hypertension.

mucosal damage in mice with PHT (Fig. 6F). Similarly, oxamic acid sodium reversed the morphological changes and increased the relative cell viability of GES-1 cells under hypoxic conditions (Fig. 6G). It is therefore concluded that the mitochondrial oxidative stress that follows PHT-mediated hypoxia impairs ATP production while contributing to increases in ROS production and LDHA-mediated lactic acid, thus promoting mucosal epithelial injury in the PHG (Fig. 7).

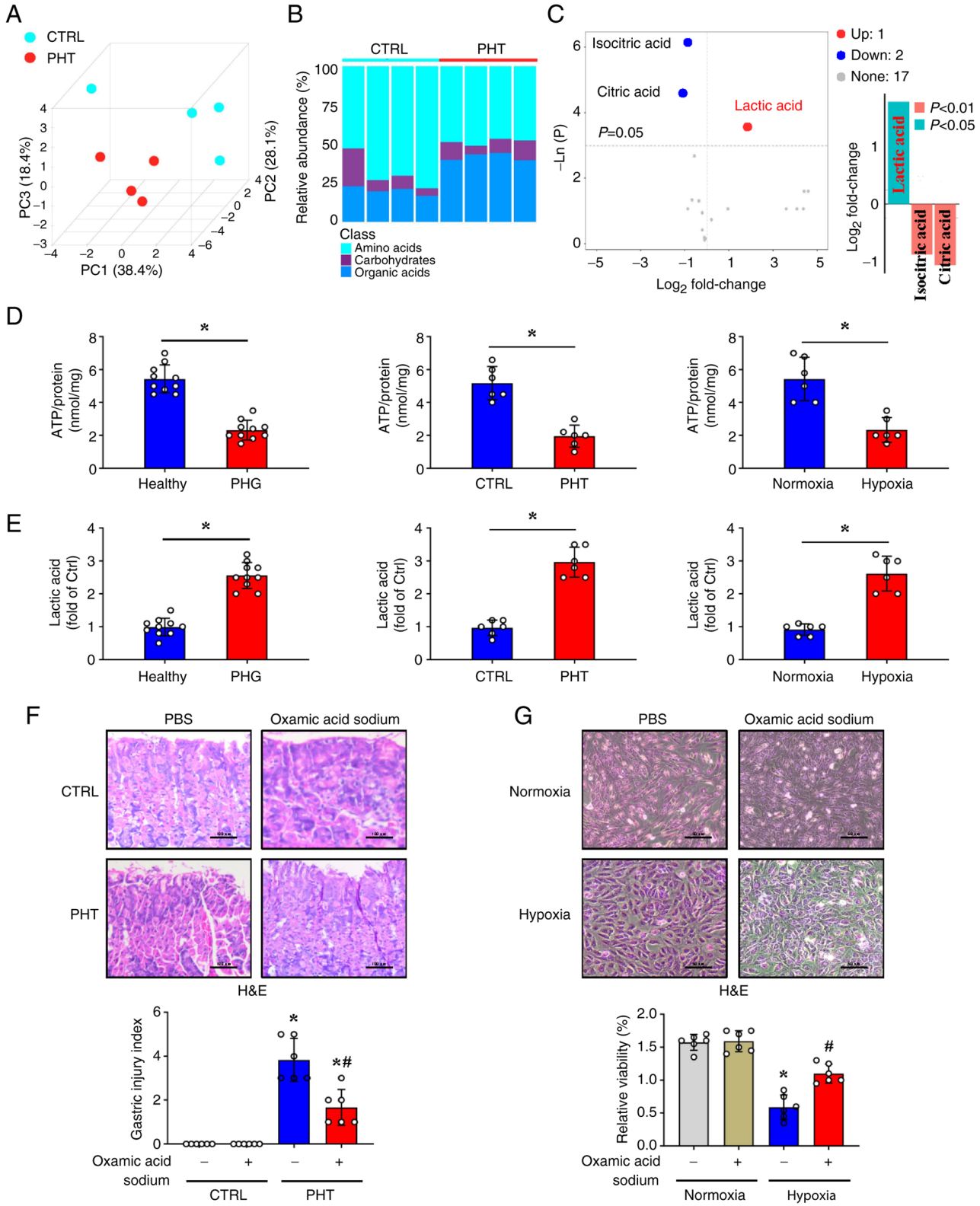

Figure 6. Mitochondrial oxidative stress in PHG is accompanied by ATP production and promotes lactic acid production. (A) Principal component analysis of metabolic components in gastric mucosal tissues from the control group and mice with PHT. n=4 per group. (B) Stacked bar plots comparing the relative abundance of amino acid metabolism, carbohydrate metabolism, and organic acid metabolism in the gastric mucosal tissues between the control group and PHT mice. (C) Volcano plot and bar chart analyses of carbohydrate metabolism biomarkers in the indicated gastric mucosal tissues. (D) The ATP concentrations in the clinical tissue samples (n=10 per group), murine models (n=6 per group), and cellular hypoxia models (n=6 per group) were analyzed. *P<0.05. (E) The lactic acid concentrations in clinical tissue samples (n=10 per group), mouse models (n=6 per group), and cellular hypoxia models (n=6 per group) were assessed. *P<0.05. (F) H&E staining and gastric mucosal injury index scores in the indicated mouse models (treated with lactate dehydrogenase A inhibitor oxamic acid sodium or not) were determined. Scale bar, 100 μm. n=6 per group. *P<0.05 vs. the control group; #P<0.05 vs. the PHT group without oxamic acid sodium. (G) H&E staining of the GES-1 cell models under normoxia and hypoxia following oxamic acid sodium administration. Cell viability from the indicated groups was also analyzed by Cell Counting Kit-8 assay. Scale bar, 50 μm. n=6 per group. *P<0.05 vs. the normoxia group; #P<0.05 vs. the hypoxia group without oxamic acid sodium. PHG, portal hypertensive gastropathy; PHT, portal hypertension; H&E, hematoxylin and eosin; CTRL, control; PBS, phosphate-buffered saline.

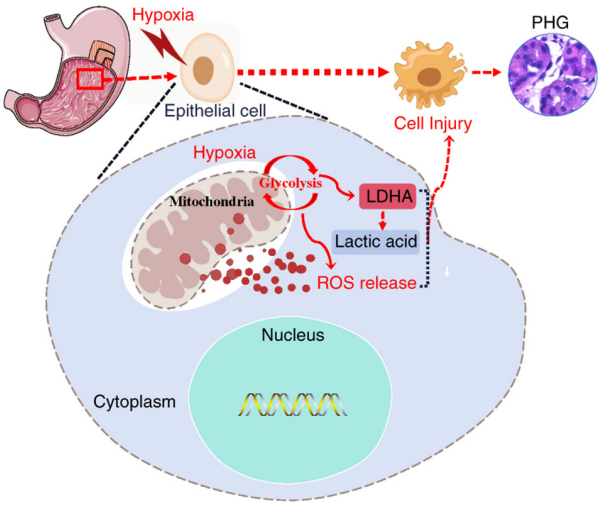

Figure 7. Schematic diagram of mitochondrial oxidative stress following hypoxia in the gastric mucosal epithelial injury of PHG. The graphical abstract is shown. PHG, portal hypertensive gastropathy; LDHA, lactate dehydrogenase A; ROS, reactive oxygen species.

Discussion

PHG represents a significant complication of both cirrhotic and noncirrhotic PHT (1). The condition is clinically defined by a portal pressure gradient exceeding 5 mmHg, measured as the pressure differential between the portal vein and hepatic veins (16). In cirrhotic cases, this haemodynamic alteration primarily stems from architectural distortion of the hepatic parenchyma and subsequent intrahepatic vascular resistance. PHT disrupts blood flow and leads to tissue hypoxia, which compromises mitochondrial integrity and triggers downstream metabolic dysregulation to exacerbate the gastric mucosal epithelial injury; the PHT-related PHG gastric mucosal lesions are commonly defined as complications in patients with PHT (5). PHG imposes a significant burden on health care systems and substantially reduces the quality of life of patients. Prior studies have demonstrated that hypoxia stabilizes hypoxia-inducible factor-1α (HIF-1α), increasing its transcriptional activity and promoting disease progression in gastric cancer and other related disorders (12,17,18). Hypoxia is closely linked to gastric mucosal damage and serves as a hallmark of gastric mucosal pathologies, spanning from inflammatory reactions to malignancies (17,19). Among these, PHG is the most representative benign lesion driven by hypoxia (20).

To assess the hypoxic state of the gastric mucosa in PHG induced by PHT, gastric tissue samples were collected from patients with an endoscopic diagnosis of PHG. Additionally, an experimental mouse model of PHT-associated PHG was established to investigate the underlying mechanisms involved. Using a Hypoxyprobe-1 detection kit, it was found that the hypoxic state in the gastric mucosa appeared in the gastric mucosal epithelia following PHT, and a positive association between hypoxia levels and the severity of gastric mucosal injury in mice with PHT was also observed. The oxygen concentration directly influences mitochondrial function, and mitochondria perform critical metabolic and signalling functions in nearly all eukaryotic cells (21). As oxygen-sensing organelles, mitochondria exhibit functional impairment and structural damage in response to hypoxia, accompanied by elevated oxidative stress (12,22). Our previous data demonstrated that mitochondrial dysfunction is involved in mucosal epithelial injury and the progression of benign and malignant gastric mucosal lesions under hypoxic conditions (14). In the present study, microarray analysis was performed on biopsied gastric mucosal tissues. Microarray analysis revealed that compared with healthy controls, patients with PHG exhibited increased activation of multiple mitochondrial pathways related to structural integrity and respiratory function. During mitochondrial ATP synthesis, the electron transport chain generates ROS as metabolic byproducts. Consequently, mitochondria represent the primary endogenous source of cellular ROS, which can serve as key mediators of oxidative stress, inflammation, and tissue damage (5,14). TEM imaging confirmed that ultrastructural mitochondrial abnormalities, including reduced mitochondrial size and decreased mitochondrial cristae, were observed in the PHG mucosa. Moreover, 4-HNE expression was significantly elevated in PHG tissues, accompanied by increased MitoSox signalling in primary gastric epithelial cells isolated from PHG sections. A PHT mouse model and a hypoxia-induced GES-1 cell model were also established, and it was verified that a significant alteration in mitochondrial structure associated with increased mitochondrial oxidative stress and ROS levels (as assayed by MitoSox staining, ROS detection, 4-HNE expression and mt 8-OHdG concentration) was observed in both the gastric mucosal epithelial cells of mice with PHT and the hypoxia-treated GES-1 cells. The progressive accumulation of mitochondrial ROS induces oxidative damage to cellular macromolecules, including DNA, proteins, and lipids. These ROS-mediated modifications can trigger diverse pathological cascades, with the magnitude and nature of their effects being modulated by microenvironmental conditions (23). Therefore, antioxidants may have specific therapeutic effects under various conditions to alleviate disease progression. Mito-TEMPO, a mitochondrion-targeted ROS scavenger, exhibits potent antioxidant activity because it selectively accumulates within mitochondria at concentrations several-fold higher than those in the cytosol. This compound attenuates mitochondrial oxidative stress by suppressing superoxide generation, thereby restoring mitophagy and counteracting excessive mitochondrial fission (22,24,25). In a PHT mouse model and an *in vitro* cell model, it was demonstrated that Mito-TEMPO administration attenuated gastric mucosal injury in mice with PHT and hypoxia-induced GES-1 cell damage, suggesting that mitochondrial oxidative stress-derived ROS resulted in gastric mucosal injury and cell damage following hypoxia. Our aforementioned findings indicate that mitochondrial structural derangements and oxidative stress escalation in the gastric mucosa drive PHG pathogenesis.

Mitochondria serve as critical hubs for numerous essential cellular processes, such as amino acid and fatty acid metabolism, the citric acid cycle, nitrogen metabolism, and oxidative phosphorylation, which generate the majority of cellular ATP. Glycolysis represents a fundamental metabolic pathway mediated by multiple glycolytic enzymes in mammalian cells. Emerging evidence indicates that gastric mucosal disorders upregulate glycolytic flux under hypoxic

conditions to sustain cellular energy homeostasis (26,27). Our microarray and metabolic pathway analyses demonstrated significant activation of glycolysis in the gastric mucosa of patients with PHG, with LDHA serving as the critical rate-limiting regulator of this process. LDHA, a key enzyme in glycolysis that is upregulated in various gastrointestinal diseases, converts pyruvate to lactic acid and produces nicotinamide adenine dinucleotide (28). Consistent with these findings, the protein expression of LDHA was also increased in gastric mucosal tissue samples from clinical PHG specimens, mouse PHT models and hypoxia-induced GES-1 cells, suggesting that mitochondrial oxidative stress drives LDHA-mediated glycolytic adaptation to bioenergetic stress under hypoxia in PHG. Various studies have suggested that in hypoxic tumour microenvironments, cancer cells undergo metabolic reprogramming to preferentially utilize glycolysis for ATP generation, enabling sustained proliferation under oxygen-deprived conditions. This glycolytic shift not only promotes tumour cell survival but also facilitates rapid biomass accumulation, thereby driving aggressive tumour progression (29). On the basis of our current data, it is suggested that increased LDHA-mediated glycolysis in the PHG, a representative disease of benign gastric lesions, aggravates mucosal injury and cell damage rather than inducing cell survival. Our previous study confirmed that HIF-1α can upregulate the expression level of LDHA, increase glycolytic metabolism, and increase mitochondrial oxidative stress, thereby participating in the occurrence and development of PHG (14). Multiple studies have shown that influenza A virus (WSN strain) impairs mitochondria, which then generates ROS, thereby stabilizing HIF-1α and activating glycolysis to provide energy for viral replication. Rabies virus glycoprotein-engineered extracellular vesicles (deliver miR-137 and downregulate HIF-1α by targeting Toll-like receptor 4 to inhibit the NF-κB pathway, thereby improving glycolytic abnormalities and neuroinflammation in autism model mice. Under glutamine deprivation, extracellular cyclophilin B in glioblastoma binds to CD147 to activate p-AKT, which upregulates HIF-1α to increase glycolysis and inhibit mitochondrial function. In acute pancreatitis, increased activity of xanthine oxidase (XO) generates ROS to activate HIF-1α, which promotes lactate accumulation via LDHA and triggers NOD-like receptor protein 3 inflammatory responses, while the inhibition of XO can alleviate pancreatic necrosis (30-33). These findings confirm that mitochondrial redox stress, which is involved in various diseases, can regulate the protein level of HIF-1α, thereby modulating the expression of related proteins such as LDHA, mediating changes in glycolytic metabolism, and participating in the occurrence and development of diseases. An in-depth exploration of the specific molecular mechanisms was not performed in the present study, and the definite association between the upregulation of LDHA induced by energy metabolism alterations and mitochondrial dysfunction-mediated ROS production under hypoxia in the PHG warrants further investigation.

Mitochondrial oxidative phosphorylation and glycolysis constitute the two primary energy-producing pathways in mammalian cells under physiological conditions. While glycolysis serves to meet cellular energy demands, its upregulation also plays a pivotal role in generating metabolic intermediates required for macromolecular biosynthesis, particularly in highly proliferative cells such as malignant cells (34). Although aerobic glycolysis (the Warburg effect) can increase ATP production to sustain energy homeostasis and supplement the tricarboxylic acid (TCA) cycle, excessive glycolytic flux in the gastric mucosal epithelium of patients with PHG can disrupt normal aerobic respiration. This metabolic reprogramming ultimately results in diminished net ATP yield despite increased glycolytic activity (14). As a glycolytic enzyme, LDHA promotes the release of glycolysis and lactic acid, and excessive lactic acid influences the immune microenvironment, intracellular signalling, cellular function and homeostasis to promote cell damage and even death (35,36). Furthermore, our metabolic profiling of gastric mucosal epithelial cells from mice with PHT revealed significant alterations in metabolic pathways, characterized by increased organic acid metabolism and decreased carbohydrate metabolism. Consistent with these findings, elevated LDHA expression and concomitant increases in lactic acid concentrations across multiple experimental systems, including clinical PHG specimens, PHT mouse models, and hypoxia-exposed GES-1 cells, were observed. These observations are particularly noteworthy given that LDHA has emerged as a promising therapeutic target in oncology. Several small-molecule LDHA inhibitors have been developed to specifically block the lactate dehydrogenase activity of LDHA, thereby suppressing glycolytic flux and inhibiting tumour progression in various cancers (37). Notably, in the present study, it was found that the LDHA inhibitor oxamic acid sodium not only alleviated gastric mucosal damage in mice with PHT but also restored morphological changes and increased relative cell viability in GES-1 cells under hypoxic conditions. The present study focused primarily on the role of LDHA in mitochondrial oxidative stress in the PHG, but metabolic reprogramming affecting mitochondrial function is complex, with other key glycolytic enzymes, such as HK2 and PKM2, also regulating cellular redox balance and mitochondrial stress. HK2 normally binds to the voltage-dependent anion channel (VDAC) on the outer mitochondrial membrane to maintain mitochondrial function, and under metabolic disturbances, glucose-induced HK2 stabilization and subsequent detachment from VDAC impair mitochondrial ATP disposal, cause membrane hyperpolarization, and increase ROS levels (38). The tetrameric form of PKM2 supports glycolytic flux and mitochondrial metabolism, whereas pathological conditions induce its sulfenylation, disrupting tetramer formation, reducing activity, and impairing mitochondrial biogenesis/fusion effects, which are reversed by PKM2 activation (39). In our previous study, quantitative protein detection of HK2 and PKM2 was conducted, and it was revealed that the expression levels of HK2 and PKM2 were increased in mouse models, which were involved in the occurrence and development of PHG (14). Given their roles in metabolic disorder-induced mitochondrial damage, HK2 and PKM2 may contribute to PHG pathogenesis, warranting further investigation. In summary, the mechanisms underlying gastric epithelial cell injury in the PHG warrant further investigation. Specifically, the roles of hypoxia-induced alterations in energy metabolism and mitochondrial dysfunction, particularly their contribution to ROS production, remain to be fully elucidated.

The present study has several limitations. First, the relationships between oxidative stress and various types of programmed cell death (such as apoptosis, pyroptosis, and ferroptosis) remain unclear. Second, the mechanism through which LDHA affects epithelial cell death is not well defined, and future studies need to focus on exploring more downstream mechanisms. Third, the intervention experiments with Mito-TEMPO (for inhibiting mitochondrial oxidative stress) and oxamic acid sodium (for inhibiting LDHA) focus mainly on short-term effects. Although the current experimental design included a 16-week drug administration period, a more longer intervention study to assess their effects on the progression of PHG has yet to be conducted. This is due to time limitations and technical constraints in establishing a long-term mouse PHG model in the current research, and the selectivity and potential side effects of these agents under long-term use also remain to be further clarified. Notably, for clinical application of these two inhibitors, large-scale experimental verification is still needed to investigate potential side effects and confirm their clinical applicability.

In summary, PHT leads to congestion and hypoxia in the gastric mucosal epithelium, and this hypoxia induces mitochondrial oxidative stress and ROS production, which are associated with abnormal glycolytic metabolism and increased LDHA-mediated lactic acid production. Ultimately, these changes result in gastric mucosal epithelial injury to promote the progression of PHG (Fig. 7).

Acknowledgements

We thank the Institutional Animal Care and Use Committee of South China Agricultural University (Guangzhou, P.R. China) for providing mice breeding and experimental studies in this experiment. We also thank the Institutional Animal Care and Use Committee of the Third Affiliated Hospital of Sun Yat-sen University (Guangzhou, P.R. China) for providing mouse experimental studies and technical support in this experiment.

Funding

The present study was supported by grants from the National Natural Science Foundation of China (grant nos. 82170569 and 82470589), and the Science and Technology Planning Projects of Guangzhou City (grant no. 2025A03J3193).

Availability of data and materials

The data generated in the present study may be requested from the corresponding author. Datasets from this study are available in the public database Science Data Bank (ScienceDB) at https://www.scidb.cn/detail?dataSetId=59ef752d1c60447a978aa3a62ad83c44.

Authors' contributions

JL performed the mouse experiments and analyzed the data of the patients. KX contributed essential reagents and conducted the cell experiments. XO planned and conducted primary cell isolation and signalling pathway study. ST designed the whole project, supervised the research and wrote the paper. JL and KX confirm the authenticity of all the raw data. All authors read and approved the final manuscript.

Ethics approval and consent to participate

The study protocol was approved [approval no. (2021)02-176] by the Clinical Research Ethics Committee of the Third Affiliated Hospital of Sun Yat-Sen University (Guangzhou, P.R. China). Written informed consent from the patients was waived. All animal experimental studies were approved (approval no. 2022F122) by the Institutional Animal Care and Use Committee of South China Agricultural University (Guangzhou, P.R. China).

Patient consent for publication

Not applicable.

Competing interests

The authors declare that they have no competing interests.

References

1. Cubillas R and Rockey DC: Portal hypertensive gastropathy: A review. Liver Int 30: 1094-1102, 2010.
2. McCormack TT, Sims J, Eyre-Brook I, Kennedy H, Goepel J, Johnson AG and Triger DR: Gastric lesions in portal hypertension: Inflammatory gastritis or congestive gastropathy? Gut 26: 1226-1232, 1985.
3. Guixé-Muntet S, Quesada-Vázquez S and Gracia-Sancho J: Pathophysiology and therapeutic options for cirrhotic portal hypertension. Lancet Gastroenterol Hepatol 9: 646-663, 2024.
4. Urrunaga NH and Rockey DC: Portal hypertensive gastropathy and colopathy. Clin Liver Dis 18: 389-406, 2014.
5. Tan SW: Molecular mechanism of portal hypertensive gastropathy: An update. Clin Res Hepatol Gastroenterol 48: 102423, 2024.
6. Luo Z, Tian M, Yang G, Tan QR, Chen YB, Li G, Zhang QW, Li YK, Wan P and Wu JG: Hypoxia signaling in human health and diseases: Implications and prospects for therapeutics. Signal Transduct Target Ther 7: 218, 2022.
7. Yuan XY, Ruan W, Bobrow B, Carmeliet P and Eltzschig HK: Targeting hypoxia-inducible factors: Therapeutic opportunities and challenges. Nat Rev Drug Discov 23: 175-200, 2024.
8. Lee P, Chandel NS and Simon MC: Cellular adaptation to hypoxia through hypoxia inducible factors and beyond. Nat Rev Mol Cell Biol 21: 268-283, 2020.
9. Brooks GA: Lactate as a fulcrum of metabolism. Redox Biol 35: 101454, 2020.
10. Sies H: Oxidative stress: A concept in redox biology and medicine. Redox Biol 4: 180-183, 2015.
11. Kierans SJ and Taylor CT: Glycolysis: A multifaceted metabolic pathway and signaling hub. J Biol Chem 300: 107906, 2024.
12. Xiao YL, Zhang YW, Xie KD, Huang XL, Liu XZ, Luo JJ and Tan SW: Mitochondrial dysfunction by FADDosome promotes gastric mucosal injury in portal hypertensive gastropathy. Int J Biol Sci 20: 2658-2685, 2024.
13. Tan S, Chen X, Xu M, Huang X, Liu H, Jiang J, Lu Y, Peng X and Wu B: PGE2/EP4 receptor attenuated mucosal injury via β-arrestin1/Src/EGFR-mediated proliferation in portal hypertensive gastropathy. Br J Pharmacol 174: 848-866, 2017.
14. Xiao YL, Liu XZ, Xie KD, Luo JJ, Zhang YW, Huang XL, Luo JN and Tan SW: Mitochondrial dysfunction induced by HIF-1α under hypoxia contributes to the development of gastric mucosal lesions. Clin Transl Med 14: e1653, 2024.
15. Tan S, Li L, Chen T, Chen X, Tao L, Lin X, Tao J, Huang X, Jiang J, Liu H and Wu B: β-Arrestin-1 protects against endoplasmic reticulum stress/p53-upregulated modulator of apoptosis-mediated apoptosis via repressing p-p65/inducible nitric oxide synthase in portal hypertensive gastropathy. Free Radic Biol Med 87: 69-83, 2015.

16. Gana JC, Cifuentes LI, Gattini D, Villarroel Del Pino LA, Peña A and Torres-Robles R: Band ligation versus beta-blockers for primary prophylaxis of oesophageal variceal bleeding in children with chronic liver disease or portal vein thrombosis. Cochrane Database Syst Rev 9: CD010546, 2019.
17. Noto JM, Piazuelo MB, Romero-Gallo J, Delgado AG, Suarez G, Akritidou K, Girod Hoffman M, Roa JC, Taylor CT and Peek RM Jr: Targeting hypoxia-inducible factor-1 alpha suppresses *Helicobacter pylori*-induced gastric injury via attenuation of both cag-mediated microbial virulence and proinflammatory host responses. Gut Microbes 15: 2263936, 2023.
18. Lin ZH, Song JL, Gao YK, Huang SH, Dou RZ, Zhong PY, Huang GQ, Han L, Zheng JS, Zhang XY, *et al*: Hypoxia-induced HIF-1α/lncRNA-PMAN inhibits ferroptosis by promoting the cytoplasmic translocation of ELAVL1 in peritoneal dissemination from gastric cancer. Redox Biol 52: 102312, 2022.
19. He C, Wang LB, Zhang JT and Xu H: Hypoxia-inducible microRNA-224 promotes the cell growth, migration and invasion by directly targeting RASSF8 in gastric cancer. Mol Cancer 16: 35, 2017.
20. Zhang YF, Lu HW, Ji H and Li YM: p53 upregulated by HIF-1α promotes gastric mucosal epithelial cells apoptosis in portal hypertensive gastropathy. Dig Liver Dis 55: 81-92, 2023.
21. Winter JM, Yadav T and Rutter J: Stressed to death: Mitochondrial stress responses connect respiration and apoptosis in cancer. Mol Cell 82: 3321-3332, 2022.
22. Fuhrmann DC and Brüne B: Mitochondrial composition and function under the control of hypoxia. Redox Biol 12: 208-215, 2017.
23. Zhang BY, Pan CY, Feng C, Yan CQ, Yu YJ, Chen ZL, Guo CJ and Wang XX: Role of mitochondrial reactive oxygen species in homeostasis regulation. Redox Rep 27: 45-52, 2022.
24. Yang SG, Bae JW, Park HJ and Koo DB: Mito-TEMPO protects preimplantation porcine embryos against mitochondrial fission-driven apoptosis through DRP1/PINK1-mediated mitophagy. Life Sci 315: 121333, 2023.
25. Shetty S, Kumar R and Bharati S: Mito-TEMPO, a mitochondria-targeted antioxidant, prevents N-nitrosodiethylamine-induced hepatocarcinogenesis in mice. Free Radic Biol Med 136: 76-86, 2019.
26. Liu X, Wang X, Zhang J, Lam EK, Shin VY, Cheng AS, Yu J, Chan FK, Sung JJ and Jin HC: Warburg effect revisited: An epigenetic link between glycolysis and gastric carcinogenesis. Oncogene 29: 442-450, 2010.
27. Cheng CT, Kuo CY, Ouyang C, Li CF, Chung Y, Chan DC, Kung HJ and Ann DK: Metabolic Stress-induced phosphorylation of KAP1 Ser473 blocks mitochondrial fusion in breast cancer cells. Cancer Res 76: 5006-5018, 2016.
28. Yi Y, Wu MY, Chen KT, Chen AH, Li LQ, Xiong Q, Wang XR, Lei WB, Xiong GX and Fang SB: LDHA-mediated glycolysis in stria vascularis endothelial cells regulates macrophages function through CX3CL1-CX3CR1 pathway in noise-induced oxidative stress. Cell Death Dis 16: 65, 2025.
29. Kooshan Z, Cárdenas-Piedra L, Clements J and Batra J: Glycolysis, the sweet appetite of the tumor microenvironment. Cancer Lett 600: 217156, 2024.
30. Zhang YJ, Chang LF, Xin X, Qiao YX, Qiao WN, Ping JH, Xia J and Su J: Influenza A virus-induced glycolysis facilitates virus replication by activating ROS/HIF-1α pathway. Free Radic Biol Med 250: 910-924, 2024.
31. Qin Q, Li MY, Fan LL, Zeng X, Zheng DY, Wang H, Jiang YT, Ma XR, Xing L, Wu LJ, *et al*: RVG engineered extracellular vesicles-transmitted miR-137 improves autism by modulating glucose metabolism and neuroinflammation. Mol Psychiatry 30: 4072-4084, 2025.
32. Yin H, Liu Y, Dong Q, Wang HY, Yan YJ, Wang XQ, Wan XQ, Yuan GQ and Pan YW: The mechanism of extracellular Cyp B promotes glioblastoma adaptation to glutamine deprivation microenvironment. Cancer Lett 597: 216862, 2024.
33. Rong J, Han CX, Huang Y, Wang YQ, Qiu Q, Wang M, Wang SS, Wang R, Yang JQ, Li X, *et al*: Inhibition of xanthine oxidase alleviated pancreatic necrosis via HIF-1 α-regulated LDHA and NLRP3 signaling pathway in acute pancreatitis. Acta Pharm Sin B 14: 3591-3604, 2024.
34. Chelakkot C, Chelakkot VS, Shin Y and Song K: Modulating glycolysis to improve cancer therapy. Int J Mol Sci 24: 2606, 2023.
35. An S, Yao Y, Hu HB, Wu JJ, Li JX, Li LL, Wu J, Sun MM, Deng ZY, Zhang YY, *et al*: PDHA1 hyperacetylation-mediated lactate overproduction promotes sepsis-induced acute kidney injury via Fis1 lactylation. Cell Death Dis 14: 457, 2023.
36. Rabinowitz JD and Enerbäck S: Lactate: The ugly duckling of energy metabolism. Nat Metab 2: 566-571, 2020.
37. Liu J, Zhang C, Zhang TL, Chang CY, Wang JM, Bazile L, Zhang LJ, Haffty BG, Hu WW and Feng ZH: Metabolic enzyme LDHA activates Rac1 GTPase as a noncanonical mechanism to promote cancer. Nat Metab 4: 1830-1846, 2022.
38. Rabbani N, Xue M and Thornalley PJ: Hexokinase-2-linked glycolytic overload and unscheduled Glycolysis-driver of insulin resistance and development of vascular complications of diabetes. Int J Mol Sci 23: 2165, 2022.
39. Qi W, Keenan HA, Li Q, Ishikado A, Kannt A, Sadowski T, Yorek MA, Wu I, Lockhart S, Coppey LJ, *et al*: Pyruvate kinase M2 activation may protect against the progression of diabetic glomerular pathology and mitochondrial dysfunction. Nat Med 23: 753-762, 2017.